Preprints.org

Article

Not peer-reviewed version

Computational Modelling of the Temporomandibular Joint: A Finite Element Study of Bifid Condyle Fractures

Micaela Miño , Bryan Moreira , Carlos Avila , Fernanda Chavez , Olga López , Jennifer Ayala , Edgar Rivera Tapia *

Posted Date: 9 May 2026

doi: 10.20944/preprints202605.0561.v1

Keywords: temporomandibular joint; bifid mandibular condyle; finite element method; computational biomechanics; stress distribution; condylar fracture

Preprints.org is a free multidisciplinary platform providing preprint service that is dedicated to making early versions of research outputs permanently available and citable. Preprints posted at Preprints.org appear in Web of Science, Crossref, Google Scholar, Scilit, Europe PMC, OpenAlex.

Copyright: This open access article is published under a Creative Commons CC BY 4.0 license, which permit the free download, distribution, and reuse, provided that the author and preprint are cited in any reuse.

Preprints.org (www.preprints.org) | NOT PEER-REVIEWED | Posted: 9 May 2026 doi:10.20944/preprints202605.0561.v1

Disclaimer/Publisher's Note: The statements, opinions, and data contained in all publications are solely those of the individual author(s) and contributor(s) and not of MDPI and/or the editor(s). MDPI and/or the editor(s) disclaim responsibility for any injury to people or property resulting from any ideas, methods, instructions, or products referred to in the content.

Article

Computational Modelling of the Temporomandibular Joint: A Finite Element Study of Bifid Condyle Fractures

Micaela Miño [1], Bryan Moreira [2], Carlos Avila [3], Fernanda Chavez [1], Olga López [1], Jennifer Ayala [1] and Edgar Rivera Tapia [2,*]

[1] Posgrado Ortodoncia, Facultad de Ciencias de la Salud "Eugenio Espejo", Universidad UTE, Quito 170527, Ecuador

[2] Mecánica Computacional e Inteligencia Artificial Aplicada (MCIAA), Ingeniería Civil, Facultad de Ciencias de la Ingenieria e Industrias, Universidad UTE, Quito 170527, Ecuador

[3] Facultad de Ingeniería Civil y Ambiental, Escuela Politécnica Nacional, Quito 170143, Ecuador

* Correspondence: edgar.rivera@ute.edu.ec; Tel: +593-(0)-962078339

Abstract

The human temporomandibular joint requires stable kinematics for optimal function; however, structural anomalies such as the bifid mandibular condyle severely compromise this biomechanical harmony. This study aims to quantify the precise biomechanical behaviour and fracture susceptibility of the bifid condyle using patient-specific finite element analysis. A high-fidelity 3D computational model was constructed from the cone-beam computed tomography data of a patient presenting with a right bifid condyle and concurrent fracture. To establish a comparative baseline, a geometrically healthy control model was computationally derived. Both models were subjected to a simulated, physiological multiaxial masticatory load of 1000 N. The simulation revealed that while the healthy control safely dissipated forces (peak cortical von Mises stress of 62.49 MPa), the bifid morphology fundamentally disrupted load transfer. Extreme mechanical forces concentrated directly at the anomalous inter-condylar notch, generating peak equivalent von Mises stresses approaching 500 MPa and peak compressive stresses nearing 600 MPa. Furthermore, localised strain energy density at the notch peaked at 12 MPa. These internal stress magnitudes significantly exceed the ultimate yield strength of human cortical bone, providing a direct biomechanical rationale for the clinically observed fracture. This computational evidence establishes that the bifid condyle acts as a critical structural vulnerability and energy sink. Consequently, the identification of a bifid condyle warrants proactive clinical management, as even asymptomatic presentations are highly predisposed to structural fatigue and macroscopic failure.

Keywords: temporomandibular joint; bifid mandibular condyle; finite element method; computational biomechanics; stress distribution; condylar fracture

1. Introduction

The human temporomandibular joint (TMJ) represents a highly sophisticated biomechanical system, functioning as a ginglymoarthrodial joint capable of complex rotational and translational movements (Ananthan et al., 2023). As one of the most mechanically complex and frequently utilised articulations in the human body, it facilitates fundamental physiological processes such as mastication, deglutition, and articulation. Consequently, a healthy temporomandibular joint must accommodate complex, six-degrees-of-freedom kinematics. This functionality defines the TMJ as a bilateral, compound, and interdependent articulation (Valenzuela-Fuenzalida et al., 2023). The smooth execution of these multidimensional movements depends heavily on the convex, singular, elliptical morphology of the mandibular condylar head, which ensures load distribution across the

© 2026 by the author(s). Distributed under a Creative Commons CC BY license.

Preprints.org (www.preprints.org) | NOT PEER-REVIEWED | Posted: 9 May 2026 doi:10.20944/preprints202605.0561.v1

biconcave articular disc and the glenoid fossa of the temporal bone (Labib et al., 2025). This morphological precision results in a highly reproducible, stable kinematic axis encompassing six degrees of freedom (Scolaro et al., 2022). Furthermore, kinematic studies mapping the instantaneous centre of rotation reveal that the kinematic centre of a healthy condyle remains highly stable, typically located slightly posterior and superior to the palpated lateral pole (Yatabe et al., 1995). Unlike conventional synovial joints, the TMJ is tasked with executing a highly complex array of coupled rotational (hinge) and translational (gliding) movements, demanding an exquisite synergy between the mandibular condyle, the interposed fibrous articular disc, the corresponding glenoid fossa, and a vast network of masticatory musculature (Mańkowski et al., 2021). Therefore, since the convergence of stable kinematics and neuromuscular interaction is essential for functional homeostasis, preserving TMJ health is a priority to ensure the correct functions of mastication.

In contrast to the healthy TMJ, the bifid mandibular condyle (BMC) emerges as an exceptionally rare and aberrant structural anomaly, presenting with an estimated prevalence of merely 0.3% to 3.0% (Borrás-Ferreres et al., 2018; Valenzuela-Fuenzalida et al., 2023). Although its precise aetiopathogenesis remains a subject of ongoing debate—broadly dichotomised into congenital developmental defects or acquired traumatic events (Borrás-Ferreres et al., 2018)—the morphological manifestation is uniformly characterised by a complete or partial duplication of the condylar head, typically demarcated by a distinct central groove (Zengin et al., 2025). This bifurcation, which may present in either an anteroposterior or mediolateral orientation, is anatomically driven by variations in dense fibrous connective tissue that subsequently induce the infoldings of the articular disc during development [Antoniades et al., 2004; Lo, 2019].

The introduction of this atypical morphology compromises the stomatognathic system. The inherent structural irregularities of the bifid condyle critically disrupt physiological load distribution across the articular surfaces. Such biomechanical perturbations not only induce chronic temporomandibular instability but also frequently serve as a primary catalyst for severe osteoarthritic degeneration (Zengin et al., 2025). To accommodate the persistent mechanical stress of a dual-headed condyle, the surrounding joint architecture is forced into a severe pathological adaptive response; specifically, the glenoid fossa undergoes significant osseous remodelling, a process that fundamentally displaces the kinematic centre of the joint.

The prevalence of the bifid mandibular condyle has been a subject of academic debate, a discrepancy driven by the varying sensitivity of the diagnostic methodologies employed across studies (Haghnegahdar et al., 2014). For decades, the inherent limitations of two-dimensional imaging, specifically panoramic radiography (PAN), obscured both the true prevalence and the intricate structural complexity of this condition. Studies utilising PAN consistently report artificially lower prevalence figures; this underrepresentation is directly attributable to the inherent flaws of 2D projection, including magnification errors, distortion, and the problematic superimposition of the zygomatic arch and cervical vertebral column over the condylar region (Zengin et al., 2025). Consequently, this superimposition of adjacent anatomical structures frequently masked the dual-headed nature of the anomaly, regularly leading to clinical misdiagnoses such as simple condylar fractures or neoplastic tumours.

The emergence of three-dimensional imaging tools, primarily Computed Tomography (CT) and Cone Beam Computed Tomography (CBCT), has altered the morphological understanding of the BMC. In contrast to 2D techniques, 3D imaging facilitates the precise spatial visualisation of the condyle across axial, coronal, and sagittal planes, revealing the true morphology of the bifid heads (Zengin et al., 2025). Furthermore, high-resolution micro-CT evaluations have exposed profound microarchitectural compromises within the BMC. These quantitative analyses reveal a significantly reduced cortical volume, a lower absolute bone volume fraction (BV/TV), and an expanded trabecular separation when compared to a healthy joint (Torres-Villar et al., 2025).

Although literature now details the gross morphological and microstructural characteristics of the BMC, the mechanical behaviour of this aberrant anatomical structure is not fully understood.

© 2026 by the author(s). Distributed under a Creative Commons CC BY license.

Preprints.org (www.preprints.org) | NOT PEER-REVIEWED | Posted: 9 May 2026 doi:10.20944/preprints202605.0561.v1

Therefore, there remains a distinct absence of robust evidence delineating the precise mechanical response of the BMC, specifically in terms of quantifiable stress and strain distributions.

To overcome the limitations of clinical imaging when evaluating the structural response of the bifid mandibular condyle under physiological loading, the Finite Element Method (FEM) provides a vital, non-invasive, and human-specific alternative. It is the 'gold-standard' computational methodology for predicting the complex biomechanical behaviour of both soft and hard tissues within the human mandible and temporomandibular joint (Mańkowski et al., 2021).

FEM operates by discretising continuous anatomical structures into a finite number of manageable sub-domains, or elements. This process allows the precise numerical calculation of strain, stress, and displacement distributions across the joint complex under specific, user-defined scenarios (Shu et al., 2021a). The accuracy of any FEM simulation rests upon three core mathematical pillars: the resolution of the geometric mesh, the assignment of accurate material properties, and the replication of physiological boundary and loading conditions.

Within morphologically normal mandibles, the application of these has yielded critical physiological and clinical insights. Simulations of axial loading directed along the natural condylar trajectory demonstrate that maximal von Mises stress concentrations occur at the narrow condylar neck. In healthy models, the threshold for macroscopic fracture initiation is measured at 1895 ± 393 N of compressive load and 3.1 ± 0.6 mm of linear displacement (Zhao et al., 2025).

Longitudinal computational tracking quantifies the phenomenon of stress shielding and its impact on post-operative condylar remodelling. FEM demonstrates that at Week 0 post-fixation, the equivalent stress on rigid titanium hardware is 7 to 9 times greater than at Week 12 (Jing et al., 2015). This stress shielding phenomenon is the primary biomechanical mechanism driving the condylar flattening, volumetric loss, and dimensional remodelling observed on follow-up CBCT scans (Jing et al., 2015). This computational data validates clinical protocols recommending intermaxillary elastic traction and a strict liquid diet during the initial four weeks to reduce overall stress magnitude.

Despite these advances in evaluating cranial structures and normal temporomandibular kinematics, a gap exists regarding structural anomalies. While FEM is proven in standard morphologies, there is no published evidence, to the best of the authors' knowledge, indicating previous studies have utilised FEM to evaluate the structural and biomechanical response of the bifid mandibular condyle.

While the bifid mandibular condyle constitutes a rare structural anomaly, the integration of high-resolution, three-dimensional imaging modalities reveals a higher clinical incidence than historical radiographic data suggested. Contemporary imaging excels in static morphological diagnosis; however, it lacks the capacity to quantify the dynamic, biomechanical response of the temporomandibular joint under functional loading.

To address this gap, this study proposes the implementation of a patient-specific, in-silico Finite Element Method model of a diagnosed BMC. The aim is to elucidate the mechanisms by which physiological forces translate into asymmetric load distributions within the atypical joint architecture. Rather than introducing a novel computational framework, this research leverages established FEM principles to map the aberrant stress-strain trajectories across the compromised articulation. The central hypothesis postulates that quantifying these biomechanical deviations from physiological baselines will provide the foundational understanding required to design and develop targeted, patient-specific therapeutic interventions.

2. Methods

2.1. Geometric Acquisition and 3D Reconstruction

2.1.1. Subject Data and Ethical Framework

The computational model was derived from a high-resolution cone-beam computed tomography (CBCT) scan of a 25-year-old female diagnosed with hypermobile Ehlers-Danlos

© 2026 by the author(s). Distributed under a Creative Commons CC BY license.

Preprints.org (www.preprints.org) | NOT PEER-REVIEWED | Posted: 9 May 2026 doi:10.20944/preprints202605.0561.v1

syndrome (hEDS). Imaging was originally indicated due to joint pain and severely restricted maximum mouth opening (15.22 mm). Radiological assessment revealed a right bifid mandibular condyle with active degeneration and a concurrent fracture (Figure 1). The contralateral (left) condyle was clinically and radiographically confirmed to be morphologically intact, devoid of prior pathological or surgical compromise.

The use of anonymised patient radiographic data for the development of these computational models was conducted in strict accordance with the Declaration of Helsinki (World Medical Association, 2024). The study protocol and the utilisation of the clinical dataset were reviewed and approved by the Human Research Ethics Committee (CEISH) at Universidad UTE (Approval Number: **CEISH-UTE04-2026-026**). Informed consent for the use of diagnostic records for research purposes was obtained prior to the commencement of the study.

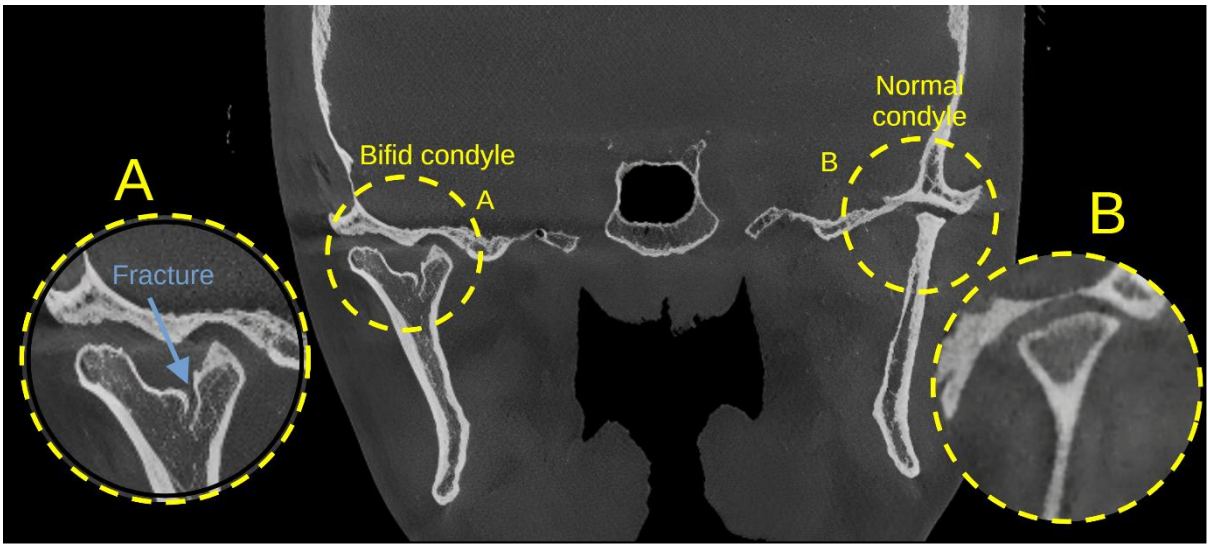

Figure 1. Coronal computed tomography imaging of the temporomandibular joint complex in a patient with hEDS, demonstrating significant structural asymmetry. (A) Detailed magnification of the right mandibular condyle, highlighting the bifid presentation and a distinct structural fracture. (B) Magnified view of the healthy, dimensionally normal left mandibular condyle, extracted from a different coronal slice depth to properly demonstrate its native morphological integrity.

2.1.2. Imaging Protocol and Data Acquisition

The CBCT imaging was specifically acquired to characterise the anomalous osteology of the bifid mandibular condyle, employing a Planmeca ProMax 3D CT scanner (Helsinki, Findland) with isotropic voxel size of 0.400 mm, The scan was acquired with a field of view of 20.0 × 17.4 cm, a tube voltage of 120 kV, a tube current of 6 mA, and an exposure time of 9.036 seconds. To preserve the precise spatial coordinates and dimensional fidelity of the craniofacial complex, the raw volumetric data was exported in the Digital Imaging and Communications in Medicine (DICOM) standard.

2.1.3. Image Processing and Segmentation

The DICOM dataset was imported into Blue Sky Plan 5 Version 5.0.27 (Libertyville, United States) for segmentation. The isolation of the relevant osseous structures, including the duplicated condylar heads, mandibular fossa, and articular eminence, was achieved employing an Automatic Jaw Segmentation protocol. This feature utilises machine learning algorithms to autonomously identify and partition distinct tissue densities—encompassing bone, teeth, nerves, and airways—directly from the volumetric data. This automated process was subsequently supplemented by manual refinement to ensure rigorous artefact reduction and precise anatomical boundary delineation.

© 2026 by the author(s). Distributed under a Creative Commons CC BY license.

Preprints.org (www.preprints.org) | NOT PEER-REVIEWED | Posted: 9 May 2026 doi:10.20944/preprints202605.0561.v1

2.1.4. Surface Generation and Mesh Export

Following segmentation, the isolated region of interest was converted into a highly resolved three-dimensional solid representation and exported as a standard tessellation language (.STL) file, thereby establishing the foundational stereolithographic mesh requisite for the subsequent reverse engineering and finite element discretisation phases.

2.2. Solid Modelling and Spatial Discretisation

2.2.1. Anatomical Refinement and Control Model Generation

Following geometric acquisition, the stereolithographic (.STL) surface mesh was directly imported into Gmsh 4.15.1 (Geuzaine and Remacle, 2009). Within this environment, the geometric mesh, representing the complex biological surfaces of the mandible, was refined to eliminate geometric anomalies. This process yielded a contiguous solid model suitable for finite element analysis. To establish a rigorous comparative baseline for evaluating the biomechanical behaviour of the anomalous joint, an in silico control model was mathematically generated (Figure 2). This comparative mandible was constructed by numerically duplicating the morphology of the contralateral, healthy condyle and mirroring it to replace the bifid articulation. This process generated a symmetrical control mandible dimensionally identical to the experimental model, isolating the bifid condyle as the sole structural variable.

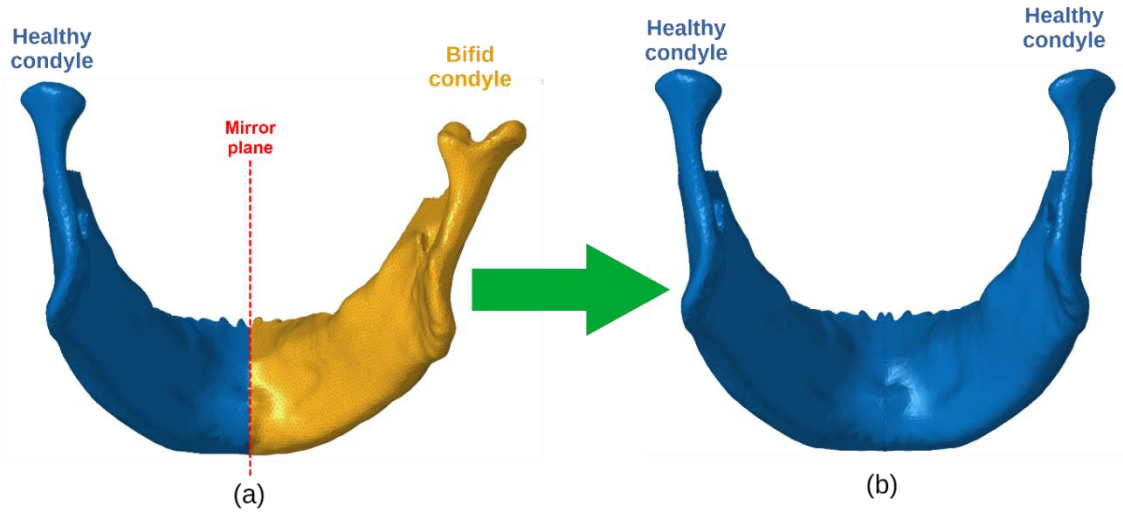

Figure 2. Computational derivation of the in silico healthy control model. The clinical case (a) displays the original 3D reconstruction of the patient's mandible, illustrating the anomalous right bifid condyle (yellow) and the native healthy left condyle (blue), separated by a mid-sagittal mirror plane. Through geometric reflection, the artificially generated control model (b) was constructed, featuring bilateral healthy condyles to serve as a structurally symmetrical baseline for biomechanical comparison.

2.2.2. Spatial Discretisation and Mesh Quality Assurance

To ensure mathematical stability and computational accuracy, the discretisation protocol prioritised the generation of a high-fidelity mesh governed by strict quality parameters (Figure 3). The integrity of the computational grid was validated against established quality thresholds to preclude numerical distortion during the finite element analysis (Burkhart et al., 2013; Rivera-Tapia et al., 2025). Specific attention was directed toward optimising the global element size, minimising average skewness, and maintaining strict controls over aspect ratio and Jacobian determinants (Table 1).

© 2026 by the author(s). Distributed under a Creative Commons CC BY license.

Preprints.org (www.preprints.org) | NOT PEER-REVIEWED | Posted: 9 May 2026 doi:10.20944/preprints202605.0561.v1

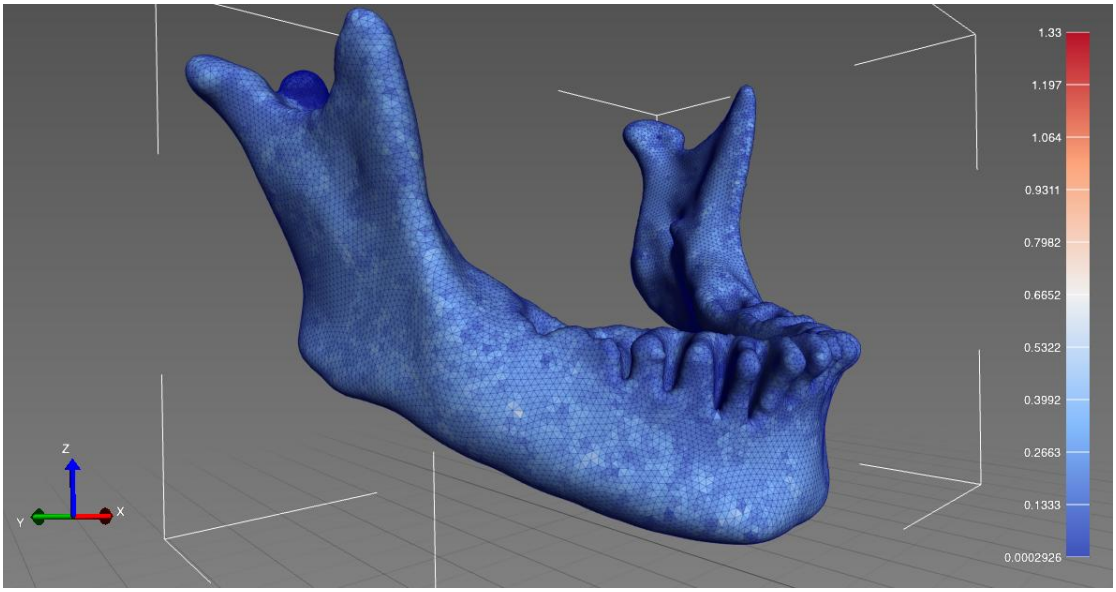

Figure 3. Distribution of Jacobian determinants across the C3D4 tetrahedral mandibular mesh. The strictly positive minimum value (0.00029) confirms the absence of negative Jacobians, validating the geometric integrity of the thin-walled cortical structures and ensuring global computational stability.

Table 1. Quantitative metrics of the spatial discretisation and mesh quality.

Parameter	Value	Acceptable Threshold
Element Type	Linear 4-node tetrahedral (C3D4), solid tetrahedrons	N/A
Global Element Size	1 mm	N/A
Bifid condyle groove element size	0.25 mm	N/A
Total Number of Elements	1336192	N/A
Total Number of Nodes	269900	N/A
Average Element Quality	1.172	>0.1
Average Aspect Ratio	1.15	< 5.0
Average Skewness	0.25	< 40°

2.3. Constitutive Material Models

To accurately represent the direction-dependent mechanical behaviour of the internal osseous tissue, both the mandibular trabecular and cortical bone regions were defined using linear, elastic, and orthotropic constitutive models (Figure 3, Table 2). The specific orthotropic properties required for this formulation—comprising Young's moduli (E_x, E_y, E_z), Poisson's ratios (ν_{xy}, ν_{xz}, ν_{yz}), and shear moduli (G_{xy}, G_{xz}, G_{yz})— were parametrised according to previously validated experimental data (Table 2, Figure 4) (Gačnik et al., 2014; Hart et al., 2017; Morgan et al., 2018).

Spatially, the entire osseous domain was discretised utilising three-dimensional, four-node tetrahedral solid elements (C3D4). Within this computational framework, the cortical layer was explicitly modelled with a uniform volumetric thickness of 1 mm. This methodological choice addresses the severe challenges inherent in segmenting distinct cortical micro-layers from standard CBCT datasets whilst accommodating the extreme geometric complexity of the craniofacial architecture. Enforcing this 1 mm thickness across the cortical continuum prevents severe mesh distortion within thin-walled regions, thereby avoiding the generation of negative Jacobians and ensuring robust computational convergence throughout the finite element analysis.

© 2026 by the author(s). Distributed under a Creative Commons CC BY license.

Preprints.org (www.preprints.org) | NOT PEER-REVIEWED | Posted: 9 May 2026 doi:10.20944/preprints202605.0561.v1

Table 2. Mechanical properties of the mandibular trabecular and cortical bone (Falcinelli et al., 2023; Gačnik et al., 2014; Mańkowski et al., 2021; Morgan et al., 2018; Öhman-Mägi et al., 2021).

Property	*Property Direction*	*Trabecular*	*Cortical*
Density (kg/m³)	*r*	*500*	*1,900*
Young's Modulus (MPa)	E_x	*1148*	*12,510*
	E_y	*1148*	*19,750*
	E_z	*210*	*10,630*
Shear Modulus (MPa)	G_{xy}	*434*	*5,840*
	G_{xz}	*68*	*4,850*
	G_{yz}	*68*	*3,890*
Poisson's Ratio	n_{xy}	*0.322*	*0.226*
	n_{xz}	*0.055*	*0.246*
	n_{yz}	*0.055*	*0.313*
Max Compressive strength (MPa)*	$(s_c)_{max}$	*3.9±2.7*	*159*
Max Tensile strength (MPa)*	$(s_c)_{max}$	*2.23±0.76*	*72*

Note: * Maximum compressive and tensile strength is applied as a mean isotropic value, providing a representative threshold to evaluate ultimate bone resistance and assess fracture risk.

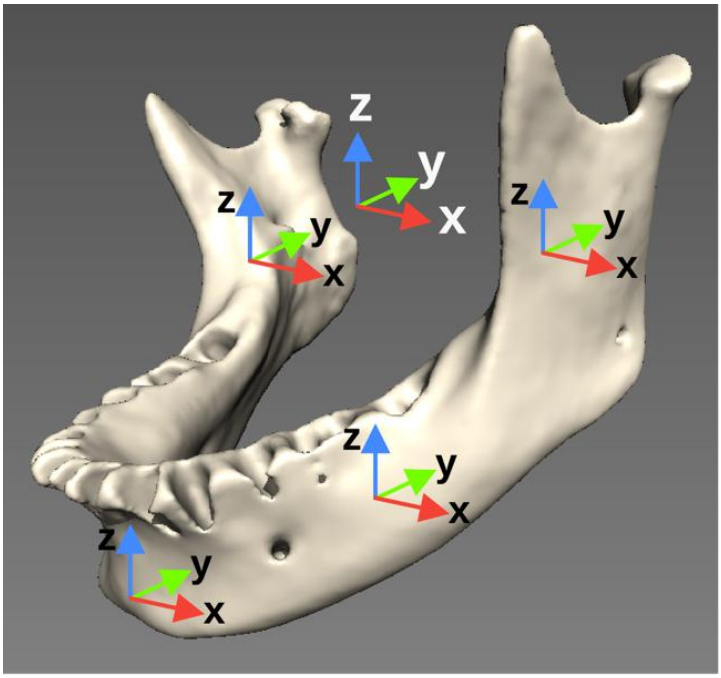

Figure 4. Spatial orientation of the global and local coordinate axes (X, Y, Z) mapped onto the mandibular geometry. These systems defined the principal material directions required for the application of the orthotropic constitutive model to the cortical and trabecular bone.

Because this study focused strictly on the isolated mandibular geometry, the temporal bone, cranial base, articular disc, and any restorative hardware were excluded from the computational framework.

2.4. Boundary Conditions

2.4.1. Kinematic Constraints

To accurately approximate the physiological environment during multiaxial loading and prevent rigid body motion, the computational model employed a combination of elastic supports and

© 2026 by the author(s). Distributed under a Creative Commons CC BY license.

Preprints.org (www.preprints.org) | NOT PEER-REVIEWED | Posted: 9 May 2026 doi:10.20944/preprints202605.0561.v1

kinematic constraints, wherein the TMJ was modelled as a hinge support (Figure 5). Because the TMJ's initial functional phase involves pure rotation prior to translation (Wong et al., 2016), fixing translational degrees of freedom (X, Y, and Z set to zero) while permitting rotations captures the physiological reality of the condyles being firmly seated within the glenoid fossae. This specific boundary condition is a validated approach to evaluate localised structural responses while preventing unconstrained rigid body motion (Ding et al., 2015; Zhang et al., 2023).

Conversely, the notch region of the bifid condyle was maintained free of boundary constraints, a methodological decision directly corroborated by radiological imaging evidence. To simulate the resistance of a static frontal bite during mastication, an elastic support was defined across the anterior dental surfaces. The nodes corresponding to the incisor zone were assigned a foundation stiffness of 2000 N/mm², replicating the compliant nature of the occlusal contact (Gregolin et al., 2017). Because the computational domain was strictly limited to the isolated mandibular geometry, the articular disc and complex temporomandibular joint articulation mechanics were omitted. For the healthy mandible, the condyles were assigned fixed displacement constraints to model the TMJ as a hinge support, restricting translation to accurately capture the physiological reality of the condyles being firmly seated within the glenoid fossae under quasi-static loading.

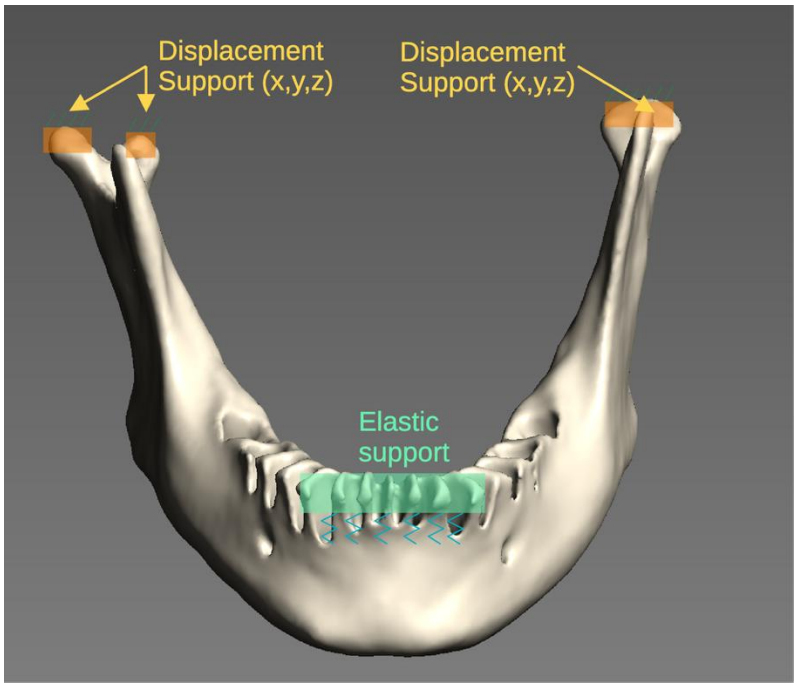

Figure 5. Hinge supports employed in the numerical model. Detail view of fixed zero-displacement constraints (orange) applied to the superior surfaces of the right bifid condyle (above) and left healthy condyle (below). Detail view of the elastic support constraint (green) applied to the anterior incisor teeth zone.

2.4.2. Physiological Muscular Loading Protocol

To replicate the in vivo mechanical environment of a critical masticatory event, a total symmetrical force of 1000 N was applied to the mandible. Rather than simulating pathological overloading, this magnitude represents the accepted upper limit of normal maximum voluntary bite force (Ding et al., 2015; Gregolin et al., 2017; Shu et al., 2021b). Utilising this physiological maximum directly influences the computational results by generating the peak expected stress and strain envelopes, thereby ensuring a conservative and robust clinical assessment of structural safety. To guarantee biofidelic load transfer, this total force was resolved into established three-dimensional vectors (Gregolin et al., 2017) and applied directly to the anatomical insertion areas of the primary elevators (Figure 6), distributing the load among the masseter (500 N), medial pterygoid (300 N), and temporalis muscles (200 N) (Table 3).

© 2026 by the author(s). Distributed under a Creative Commons CC BY license.

Preprints.org (www.preprints.org) | NOT PEER-REVIEWED | Posted: 9 May 2026 doi:10.20944/preprints202605.0561.v1

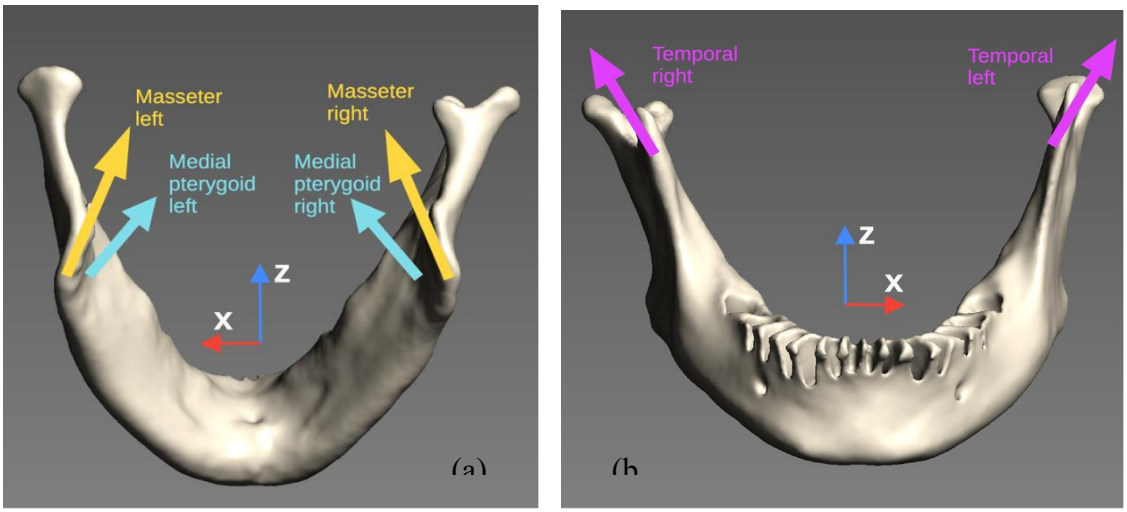

Figure 6. Location and direction of masticatory loads applied in the numerical model. (a) masseter and medial pterygoid muscles, and (b) temporal muscles.

Table 3. Physiological loading parameterisation of the mandible while mastication (Al-Ahmari et al., 2015; Gregolin et al., 2017).

Muscle Group	X-axis (N)(Medial/Lateral)	Y-axis (N)(Anterior/Posterior)	Z-axis (N)(Superior/Inferior)	Total Magnitude (N)
Masseter right	-104.7	-51.7	221.2	250
Masseter left	104.7	-51.7	221.2	250
Temporal right	50.0	22.1	83.7	100
Temporal left	-50.0	22.1	83.7	100
Medial pterygoid right	-55.8	-72.9	118.6	150
Medial pterygoid left	55.8	-72.9	118.6	150

2.5. Contact Interactions and Interface Conditions

A tied face-on-facet contact formulation rigidly bonded the 1 mm cortical layer to the internal trabecular core, ensuring structural continuity. To prevent non-physical sliding or mesh separation under muscular loading, the solver enforced this interface using a penalty method with a penalty factor of 100 and a penetration tolerance of 0.1. These specific parameters were selected to optimise computational convergence whilst strictly maintaining the physical and kinematic realism of the internal osseous boundaries.

The computational model explicitly excluded the fibrous articular disc, retrodiscal tissues, and capsular ligaments. This decision intentionally simplified the joint's complex multi-body interactions. Instead of simulating dynamic osseous contact, fixed displacement constraints applied to the superior condylar facets managed the articulation under nominally frictionless tangential behaviour. This standardised interface protocol applied uniformly across all simulated geometries. The bifid condyle's structural anomaly—including its dual heads and explicitly unconstrained central notch—required no unique multi-body interaction algorithms or modified contact definitions. Maintaining this uniform contact behaviour ensures a strictly controlled comparative baseline against the healthy mandibular model.

© 2026 by the author(s). Distributed under a Creative Commons CC BY license.

Preprints.org (www.preprints.org) | NOT PEER-REVIEWED | Posted: 9 May 2026 doi:10.20944/preprints202605.0561.v1

2.6. Model Validation and Clinical Evaluation Criteria

Evaluating the specific biomechanical impact of the bifid anomaly required the computational creation of a healthy, anatomically normative mandibular control model. Digitally reconstructing a standard, singular condylar morphology directly onto the patient's specific anatomy inherently eliminates confounding inter-patient variables, such as disparities in bone size, age, and underlying physiological conditions. This strictly controlled benchmark serves two critical scientific functions, significantly widening the clinical relevance of the research beyond a singular pathological observation.

First, this computationally generated healthy jaw establishes a highly reliable baseline for methodological validation. By systematically comparing the stress distributions and magnitudes against established in vivo and computational temporomandibular joint literature (Gregolin et al., 2017; Mańkowski et al., 2021; Zhao et al., 2025), the initial phase confirms the physiological accuracy of the global stiffness matrix, boundary conditions, and applied muscular loading protocols.

Second, to establish clinical validation of the pathological model, the computational stress distributions were spatially correlated with the patient's radiological data. Specifically, the in silico regions of peak equivalent von Mises stress (serving as a scalar indicator of structural compromise) and Principal stresses (delineating pure tensile and compressive failure modes) were mapped directly onto the macroscopic fracture morphology visualised in the patient's post-trauma CT images (Figure 1). This spatial comparison was conducted to evaluate the congruence between the mathematically induced zones of critical stress concentration and the actual in vivo fracture lines, thereby assessing the patient-specific predictive accuracy of the computational framework.

Following this rigorous validation, the post-processing phase evaluated the broader clinical implications of the structural anomaly. The computational framework quantitatively compared the stress concentrations at the pathological unconstrained central notch and dual articular heads directly against the control. This strict comparative pipeline successfully isolates the specific mechanical deviations induced solely by the structural anomaly.

3. Results

3.1. Baseline Biomechanics of the Control Model

Under muscular loading, the healthy mandibular model demonstrated an efficient and stable transfer of forces. Within the cortical shell, the equivalent von Mises stress peaked at 62.49 MPa, predominantly localising at the ramus, with visible stress concentrations extending along the anterior aspect of the condylar necks (Figure 7). As the mechanical load transferred internally, the underlying trabecular core exhibited profound stress shielding. The maximum von Mises stress within the cancellous bone dropped significantly to 1.6 MPa at the ramus (Figure 8), illustrating the cortical shell's structural capacity to absorb and dissipate functional loads before they reach the internal network.

Principal stress analysis was utilised to isolate pure tensile (σ_1) and compressive (σ_3) stress distributions across the cortical shell and underlying cancellous network (Figure 9). Within the cortical bone, peak tension (σ_1) reached 31.85 MPa, orientated primarily along the medial rami, whereas peak compression (σ_3) reached -40.6 MPa, localising at the anterior condylar necks. This robust load dissipation effectively shielded the internal trabecular compartment, which registered nominal stress magnitudes, peaking at merely 1.0 MPa in tension and -0.16 MPa in compression.

© 2026 by the author(s). Distributed under a Creative Commons CC BY license.

Preprints.org (www.preprints.org) | NOT PEER-REVIEWED | Posted: 9 May 2026 doi:10.20944/preprints202605.0561.v1

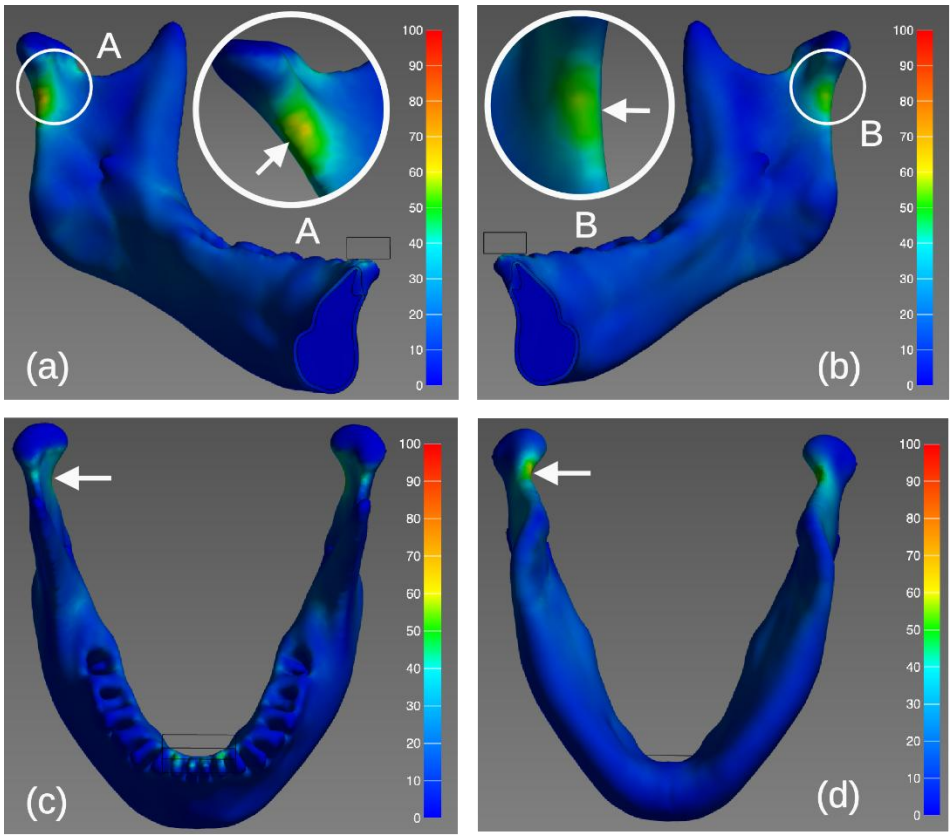

Figure 7. Cortical stress distribution across the "healthy" mandibular model under physiological loading. The colour map quantifies the equivalent von Mises stress in MPa. Magnified insets (A, B) detail the primary stress concentrations localising on the anterior aspect of the condylar necks.

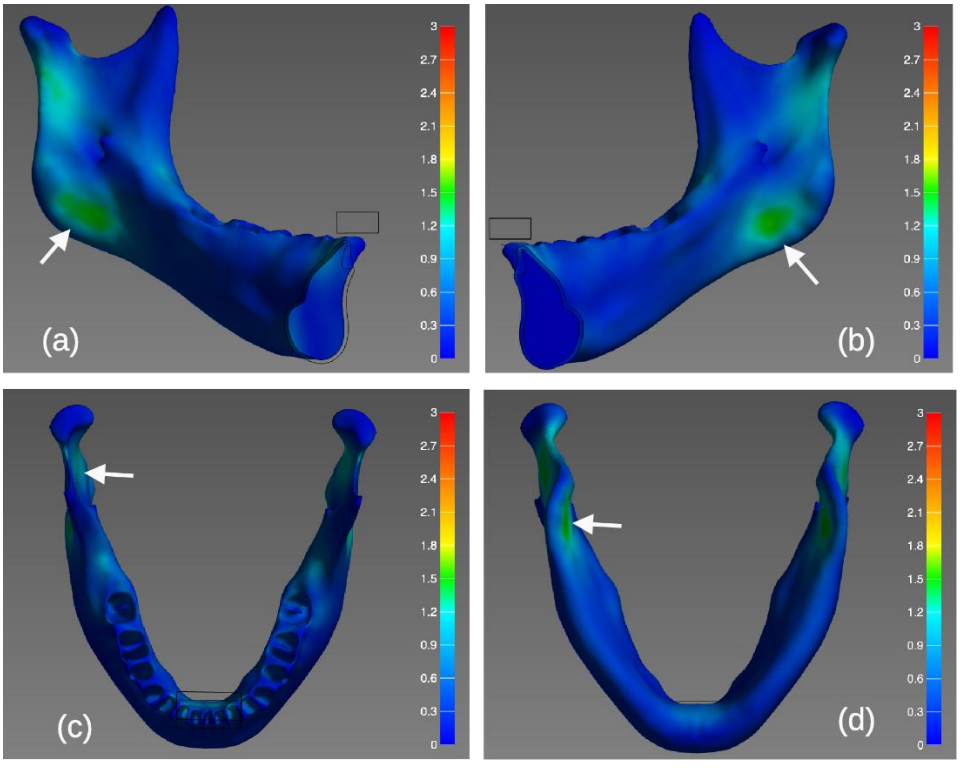

Figure 8. Internal stress distribution across the trabecular core of the healthy mandibular model under physiological loading. The colour map quantifies the equivalent von Mises stress in MPa. .

© 2026 by the author(s). Distributed under a Creative Commons CC BY license.

Preprints.org (www.preprints.org) | NOT PEER-REVIEWED | Posted: 9 May 2026 doi:10.20944/preprints202605.0561.v1

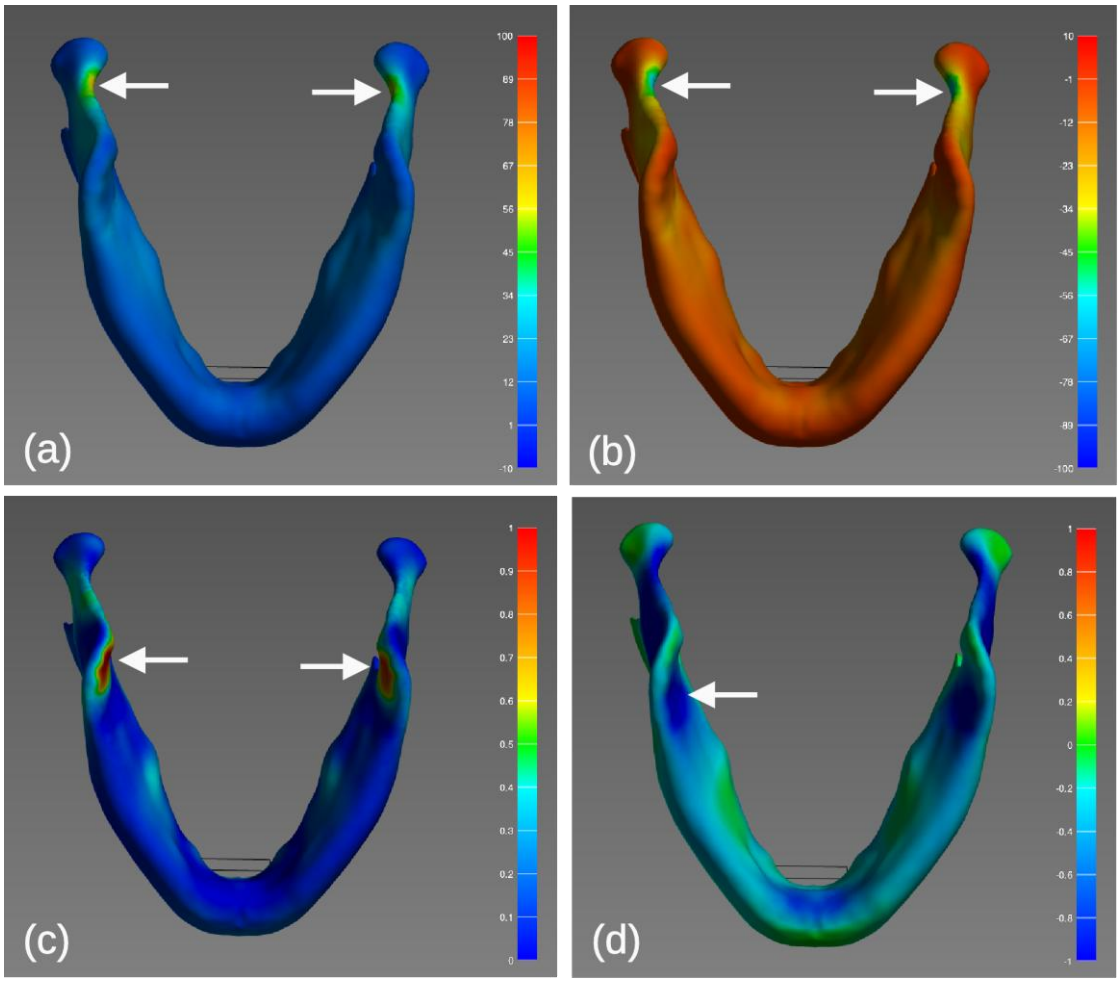

Figure 9. The 1st Principal Stress maps isolate maximum tension, demonstrating the cortical shell (a) experiencing peak tensile stresses along the medial rami, while the trabecular core (c) dissipates these loads. Conversely, the 3rd Principal Stress maps isolate maximum compression, with the cortical shell (b) absorbing peak compressive stresses at the anterior condylar necks, thereby shielding the internal trabecular network (d). Stress is quantified in MPa.

3.2. Altered Load Dissipation within the Bifid Condyle

In the pathological bifid model, the equivalent von Mises stress distribution exhibited a markedly different spatial pattern compared to the healthy baseline. Under identical physiological loading as the control group (Figures 7, 8, and 9), the induced cortical von Mises stress reached a computed maximum of approximately 500 MPa, far exceeding physiological limits. This extreme mathematical peak did not distribute along the ramus; rather, it localised as a highly concentrated focal band directly across the anomalous inter-condylar notch (Figure 10c), indicating a zone of inevitable structural collapse.

The internal trabecular core mirrored this altered spatial distribution. While the healthy cancellous bone maintained widespread low-stress shielding, the trabecular compartment of the bifid model demonstrated a peak equivalent von Mises stress of 2.6 MPa, similarly localising directly beneath the pathological notch (Figure 11c).

The evaluation of principal stress vectors provided a descriptive mapping of the tensile and compressive forces acting upon the altered anatomy (Figure 12). Within the cortical shell, the 1st Principal Stress maps revealed a maximum tensile load of 450 MPa. This peak tension was visually isolated at the anomalous notch (Figure 12a), contrasting with the more diffuse distribution seen in the intact model. The 3rd Principal Stress maps demonstrated a corresponding peak compressive force of nearly 600 MPa, converging at the exact same inter-condylar notch region (Figure 12b).

© 2026 by the author(s). Distributed under a Creative Commons CC BY license.

Preprints.org (www.preprints.org) | NOT PEER-REVIEWED | Posted: 9 May 2026 doi:10.20944/preprints202605.0561.v1

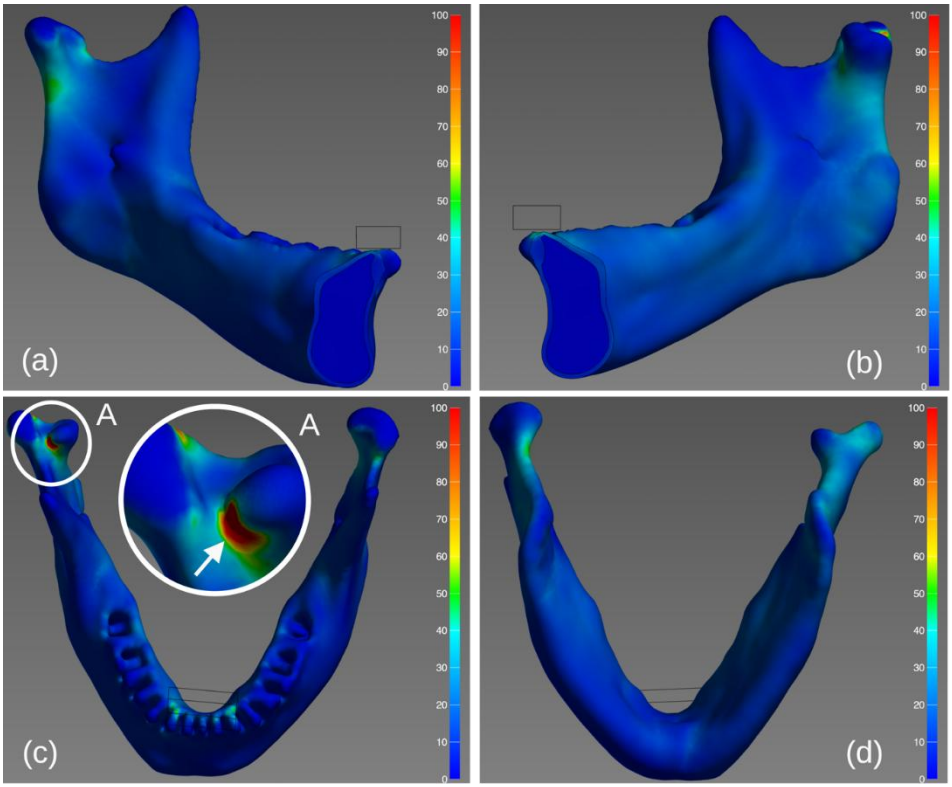

Figure 10. Equivalent von Mises stress (MPa) distribution across the cortical shell of the pathological bifid model. Panels (a)-(d) illustrate the altered mechanical load pathways. Magnified inset (A) isolates the critical stress concentration localising at the anomalous anterior inter-condylar notch.

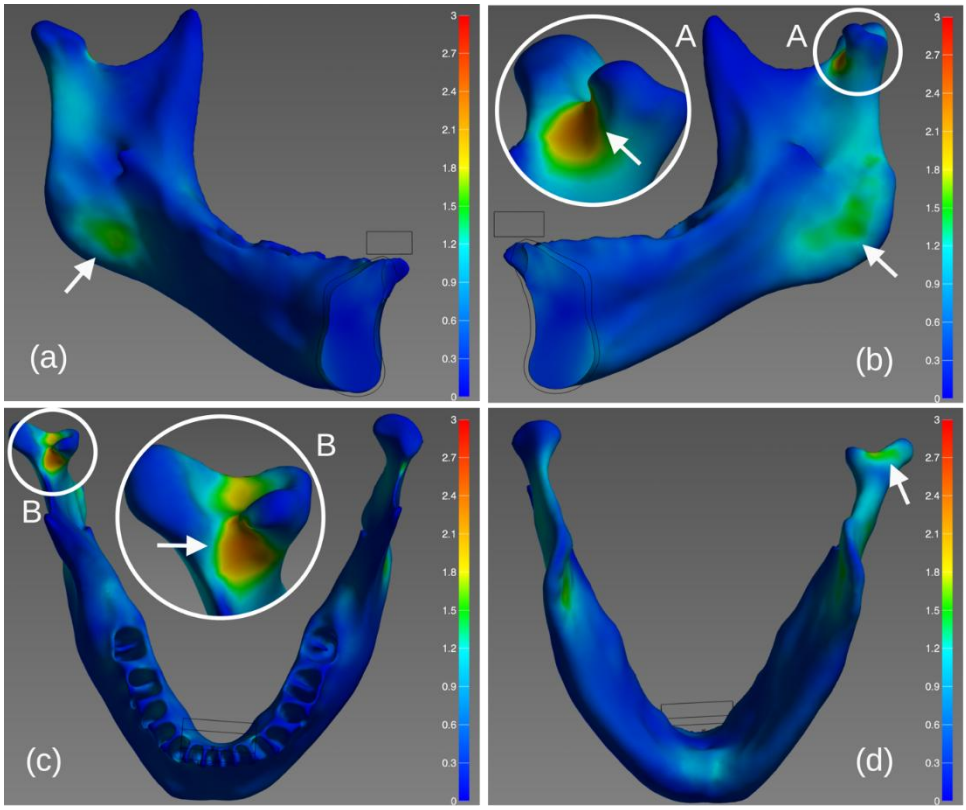

Figure 11. Equivalent von Mises stress (MPa) distribution across the internal trabecular core of the pathological bifid model. Panels (a)-(d) illustrate the altered mechanical load pathways. Magnified insets (A, B) isolate the critical stress concentrations localising at the anomalous anterior inter-condylar notch.

© 2026 by the author(s). Distributed under a Creative Commons CC BY license.

Preprints.org (www.preprints.org) | NOT PEER-REVIEWED | Posted: 9 May 2026 doi:10.20944/preprints202605.0561.v1

This focal concentration of purely tensile and compressive forces was also present within the cancellous bone. The internal trabecular network recorded a peak tensile force of approximately 2 MPa (Figure 12c) and a maximum compressive force of 2 MPa (Figure 12d), both spatially aligned with the cortical stress concentrations above them.

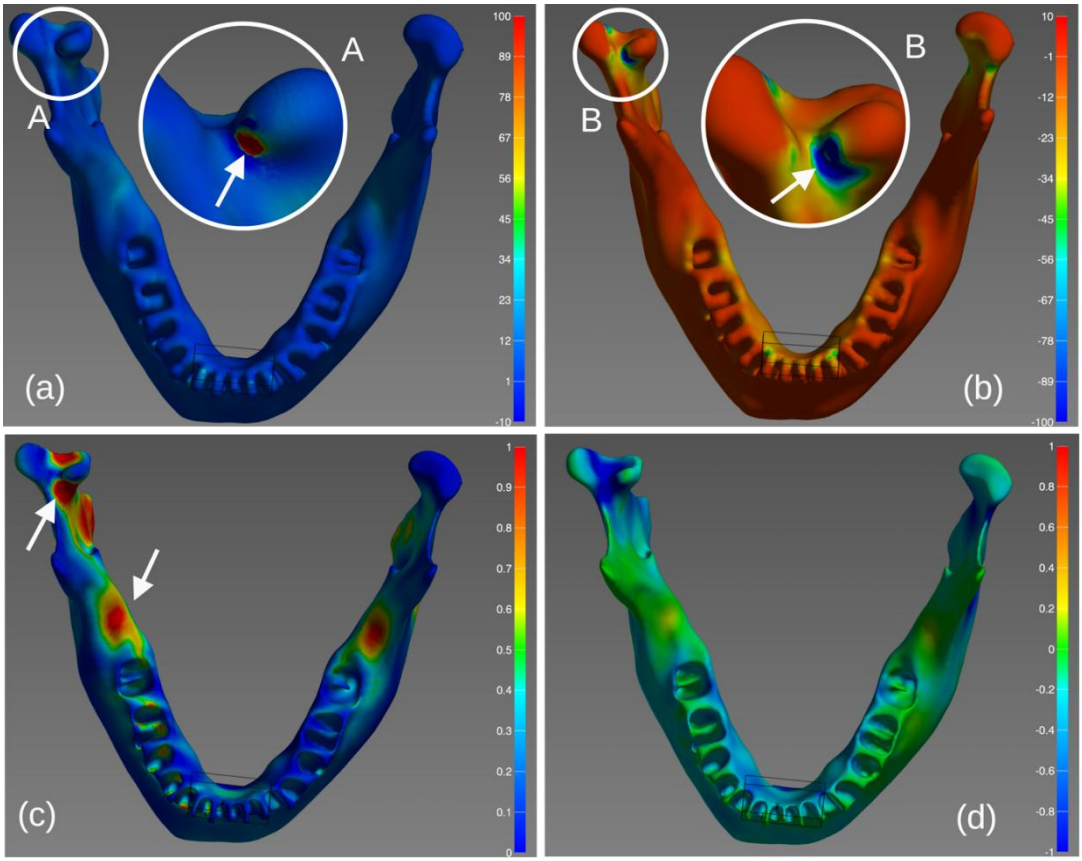

Figure 12. Principal stress (MPa) distribution across the pathological bifid model, distinguishing the cortical shell (a, b) and internal trabecular core (c, d). The 1st Principal Stress maps reveal critical tensile forces localising at the anomalous inter-condylar notch (a, inset A) and propagating internally (c). The 3rd Principal Stress maps show extreme compressive forces concentrating at the same notch (b, inset B), severely disrupting load transfer to the trabecular network (d).

3.3. Strain Energy Density Analysis

An analysis of strain energy density (SED) established the direct mechanical link between the observed stress concentrations and structural failure (Figure 13). The healthy condyle, with its smooth, intact, uncompromised geometry, was shown to efficiently and safely distribute mechanical energy across its entire structure (Figure 13b). Under physiological loading, mechanical energy was safely dissipated, resulting in uniformly low and entirely physiological SED values throughout the healthy condylar bone, visible as a predominantly blue spectrum in the colour map. In contrast, the geometrical anomaly of the bifid structure acted as a severe energy sink. The sharp pathological inter-condylar notch (Figure 13a, inset A) operated as a stress and energy concentrator. Within this anomalous region, localised strain energy density was observed to accumulate and peak at 12 MPa, represented by a localised red 'hot spot' in the map. This dramatic, localised concentration of strain energy generated internal stress levels approaching 500 MPa.

© 2026 by the author(s). Distributed under a Creative Commons CC BY license.

Preprints.org (www.preprints.org) | NOT PEER-REVIEWED | Posted: 9 May 2026 doi:10.20944/preprints202605.0561.v1

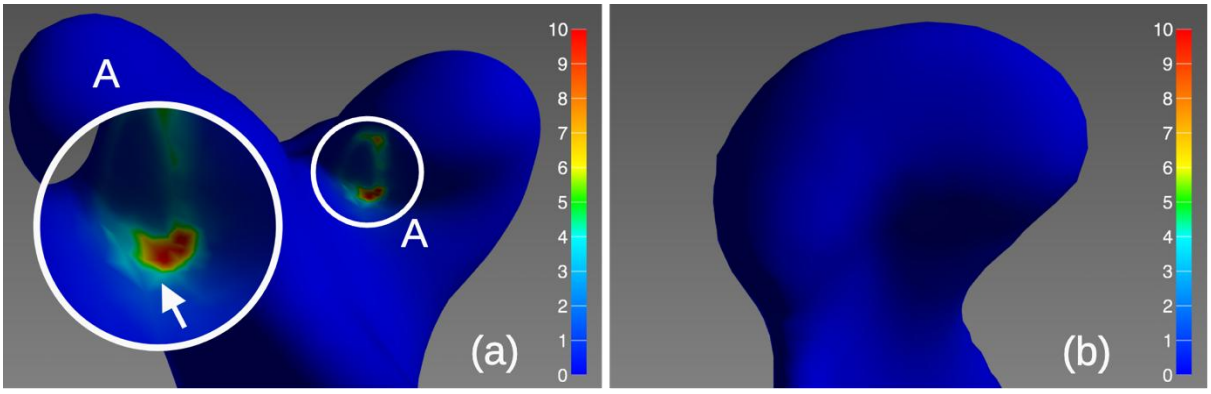

Figure 13. Strain energy density in (a) a right bifid condyle and (b) a right healthy condyle.

4. Discussion

This study developed the first finite element analysis of the bifid condyle, to the authors' knowledge, to explore the biomechanical behaviour that leads to its fracture. While previous assessments of this anomaly have predominantly relied on radiographic observation (Borrás-Ferreres et al., 2018; Haghnegahdar et al., 2014; Zengin et al., 2025), the current computational framework offers a quantitative evaluation of the internal stress distribution. To establish a comparative baseline, a healthy condyle was computationally reconstructed from the patient's own intact anatomy. This approach isolated the anomalous bifid geometry as the primary variable under investigation, aiming to control for individual physiological factors such as loading, cortical and trabecular bone and overall mandibular size.

The results suggest that the bifid condyle may act as a potential structural vulnerability that alters physiological load dissipation. Specifically, the mechanical simulations demonstrated marked stress and strain energy concentrations localising at the inter-condylar notch. These computationally predicted concentrations align with the clinical radiographic evidence of the patient's actual fracture site. This correlation provides a plausible biomechanical rationale for the structural failure, indicating that the bifid geometry may increase susceptibility to fracture under standard masticatory forces.

As demonstrated by the healthy control model, stress dissipation successfully maintains both tensile and compressive stress well within physiological thresholds (Nogueira et al., 2025; Widyastuti et al., 2026). However, the introduction of a bifid morphology fundamentally disrupts this protective mechanism (Labib et al., 2025; Zengin et al., 2025). The sharp inter-condylar notch acts as a severe stress concentrator, creating a focal point of extreme mechanical deviation. Exhibiting a localised strain energy density peaking at 12 MPa (Figure 13) and corresponding theoretical internal stresses approaching 500 MPa (Figure 10), the altered bifid anatomy induces stress concentrations that significantly exceed the ultimate compressive strength of standard human cortical bone (159 MPa, Table 2). Because the computational framework assumes linear elastic behaviour without simulating physical crack propagation, this 500 MPa magnitude represents a mathematical peak rather than a sustainable physiological state. However, this extreme magnitude serves as a robust predictive indicator of structural collapse; the computational prediction that the pathological geometry cannot withstand standard functional loading is directly validated by the clinical CT imaging (Figure 1), which exhibits macroscopic bone fracture corresponding to these high-stress regions.

Building upon this concentration of force, a distinct hypothesis regarding the initiation and propagation of the fracture can be formulated. The computational evidence suggests that the mechanical damage initiated at the regions experiencing maximal constraint, specifically corresponding to the fixed displacement zone in the model (Figure 5). This mechanical vulnerability aligns with established biomechanical principles, where maximum loading pathways within the condylar arch dictate structural failure (Sevinç Gül et al., 2025). Because the cortical shell at the notch absorbs the brunt of this extreme energy concentration, it loses its ability to shield the internal structures. Consequently, it is hypothesised that mechanical failure initiates as a distinct cortical

© 2026 by the author(s). Distributed under a Creative Commons CC BY license.

Preprints.org (www.preprints.org) | NOT PEER-REVIEWED | Posted: 9 May 2026 doi:10.20944/preprints202605.0561.v1

rupture at the fixed displacement zone, subsequently forcing the underlying trabecular network to absorb chaotic, unshielded loads. This sequential failure mechanism acts as a critical structural vulnerability, providing a direct biomechanical explanation for the clinically observed fracture of the cortical shell.

To contextualise the severity of the load dissipation in the bifid model, it is necessary to compare the stress magnitudes obtained in this study with the computational formulated healthy case. In the healthy control model, the equivalent von Mises stress within the cortical shell peaked at 62.49 MPa (Figure 7). This magnitude aligns closely with multiple independent finite element analyses of the intact mandible under physiological masticatory loading. Under simulated clenching, peak von mises stresses in the standard condylar neck region have been reported to reach approximately 40 to 60 MPa (Ding et al., 2015). Comparable healthy cortical stress distributions, ranging from 50 MPa to 80 MPa, are consistently documented under similar functional loads (Gregolin et al., 2017; Mańkowski et al., 2021) . Therefore, the physiological baseline (62.49 MPa) generated in this study closely replicates the outcomes of previous studies without reaching the max compressive strength of the cortical bone of the mandible (Gregolin et al., 2017). However, the introduction of the bifid anomaly radically altered these standard load distributions. The literature indicates that the ultimate tensile strength of human cortical bone typically falls between 100 MPa and 150 MPa (Öhman-Mägi et al., 2021), while its ultimate compressive strength is approximately 150 MPa to 200 MPa (Mańkowski et al., 2021; Sevinç Gül et al., 2025). Under identical simulated loading, the anomalous inter-condylar notch in the bifid model generated a 1st Principal Stress (tension) of 450 MPa and a 3rd Principal Stress (compression) of nearly 600 MPa. Because the local forces generated at the bifid notch exceed these established biological yield limits of cortical tissue by a factor of roughly three to four this extreme mechanical overload directly caused the condylar fracture observed in the diagnostic radiograph (Figure 1).

The clinical implications of this mechanical deviation are significant. In routine practice, the mandibular bifid condyle is frequently dismissed as a benign, incidental radiographic variant, largely because many cases do not present with acute clinical symptoms. However, the present analysis establishes that the absence of immediate symptomatology does not equate to long-term mechanical stability. Regardless of clinical presentation, the structural discontinuity acts as a critical energy sink, accumulating a peak Strain Energy Density ($U = {}^{1}/_{2}\,\sigma\epsilon$) of 12 MPa under standard muscular loading (Figure 13). Unlike healthy, congruent articulations that uniformly dissipate masticatory work across broad cortical and cancellous volumes (Chen et al., 1998), the anomalous curvature of the pathological joint disrupts physiological load transfer. This geometric irregularity induces severe stress concentrations, compelling highly localised trabecular regions to absorb elastic energy well beyond their structural transfer capacity (Carter and Hayes, 1977). Biomechanically, this pathological accumulation indicates an inability to safely dissipate functional mechanical energy, predisposing the local tissue to silent, progressive microdamage, structural fatigue, and maladaptive mechanobiological remodelling (Huiskes et al., 2000). Because this continuous cycle of microstructural degradation establishes a direct, often unobserved pathway to eventual macroscopic joint failure, the radiographic identification of a bifid morphology must be viewed from a clinical management perspective as a high-risk precursor to fracture. Translating these biomechanical stress-strain evaluations into clinical practice will provide orthodontic and maxillofacial practitioners with a definitive, evidence-based framework for the proactive monitoring and mechanical offloading of this rare condition.

While this study provides a computational framework for understanding the structural failure of the bifid condyle, several inherent methodological limitations must be acknowledged. A primary challenge in mandibular finite element modelling is the accurate computational replication of the cortical shell. The in vivo cortical layer possesses a highly irregular, anisotropic structure with significant regional variations in thickness. To ensure mathematical convergence during the finite element processing and to explicitly avoid the generation of negative volumes or highly distorted mesh elements, necessary geometric simplifications were applied to the anatomical models.

© 2026 by the author(s). Distributed under a Creative Commons CC BY license.

Preprints.org (www.preprints.org) | NOT PEER-REVIEWED | Posted: 9 May 2026 doi:10.20944/preprints202605.0561.v1

Although these surface smoothing modifications successfully enhanced overall mesh quality and computational stability, they represent an idealisation that may marginally homogenise highly localised stress responses compared to true biological conditions.

Furthermore, while the computational reconstruction of a normative healthy condyle provided a rigorous, patient-specific comparative baseline, it remains a mathematical approximation. Obtaining a genuinely identical, perfectly healthy condylar control is inherently difficult due to natural bilateral asymmetry and the broad physiological variability of mandibular behaviour. The mandible operates as a complex, dynamic system; therefore, the assumption of perfect symmetry for the control model cannot account for minor pre-existing developmental differences. Finally, while the simulations incorporated multi-axial muscular loading to represent the directional complexity of masticatory forces, the analysis was executed using a quasi-static solver. Although this is a highly robust and standard approach for comparative stress evaluation, a quasi-static assumption inherently neglects time-dependent dynamic effects—such as inertia, the strain-rate dependency of cortical bone, and cyclic fatigue—that occur during actual jaw function.

Despite these necessary simplifications, the sheer magnitude of the mechanical deviations observed at the bifid notch—exceeding physiological baselines by several orders of magnitude—provides confidence that the identified structural vulnerability remains valid regardless of minor computational standardisations.

5. Conclusions

This study highlights that the bifid mandibular condyle transcends a mere anatomical variant, representing a profound biomechanical vulnerability. By computationally replicating patient-specific kinematics, our analysis confirms that the anomalous inter-condylar notch functions as a severe mechanical energy sink. Under physiological loading, the bifid condyle concentrates tensile and compressive forces to mathematically predicted peaks approaching 500 MPa and 600 MPa, respectively. Because these localised stresses categorically exceed the ultimate compressive and tensile thresholds of human cortical bone, the anomaly fundamentally disrupts load dissipation, directly instigating structural failure.

These findings challenge the prevailing clinical paradigm that asymptomatic bifid condyle require minimal intervention. The demonstrated accumulation of pathological strain energy indicates an inherent predisposition to silent micro-damage and eventual macroscopic fracture. Therefore, clinicians must reclassify the bifid mandible condyle as a high-risk structural compromise, necessitating proactive orthopaedic monitoring and targeted mechanical offloading to prevent inevitable mechanobiological degradation.

References

Aguiar, R., & Del Castillo, F. (2019). What an inelastic flat drift slightly higher than two percent means [Graduation project]. Universidad de Fuerzas Armadas ESPE.

Anon, (2017). Normas de diseño sismo resistente 1st ed. p. Retrieved from: https://es.slideshare.net/SAAVEDRA1988/control-de-la-deriva en las-normas-de-diseño-sismo resistente.

Antoniades, K., Hadjipetrou, L., Antoniades, V., & Paraskevopoulos, K. (2004). Bilateral bifid mandibular condyle. Oral Surgery, Oral Medicine, Oral Pathology, Oral Radiology, and Endodontology, 97(4), 535-538.

Arévalo, C. (2021). Evaluación del impacto de los límites de deriva en el diseño de edificaciones en concreto reforzado con aislamiento sísmico de base. Facultad de Ingeniería Civil, Universidad de La Salle

Barros Bastidas, I., M. & Peñafiel Plazarte, m., j. (2015). Análisis comparativo económico - estructural entre un sistema aporticado, un sistema aporticado con muros estructurales y un sistema de paredes portantes, en un edificio de 10 pisos [Project prior to obtaining the degree of Civil Engineer with a specialization in Structures]. Escuela Politécnica Nacional

Barragán, A. A. & Cevallos, J. I. (2015). Análisis comparativo entre un edificio con pórticos resistentes a momentos con la inclusión de amortiguadores de masa sintonizada y un edificio con sistema dual de muros de corte [Graduation project]. Escuela Superior Politécnica del Litoral

© 2026 by the author(s). Distributed under a Creative Commons CC BY license.

Preprints.org (www.preprints.org) | NOT PEER-REVIEWED | Posted: 9 May 2026 doi:10.20944/preprints202605.0561.v1

Borrero, M. (2021). Estimación de la variabilidad de la deriva y del cortante basal resistente de pórticos de concreto reforzado en Bogotá. [Graduation project]. Pontificia Universidad Javeriana.

Bohórquez, N., & Viteri, P. (2022). Evaluación del impacto ambiental generado por la toma de decisiones en la concepción estructural de un edificio tipo de la ciudad de Quito [Project prior to obtaining the degree of Civil Engineer]. Escuela Politécnica Nacional

Campos, J. P. (2015, 15 febrero). Normativa chilena: instrumentos, actores, hitos y desafíos Estructurales, R., Biempotrado, G., Biarticulado, G., Simple, R., & Multivano, R. (n.d.). Pórtico rígido conectado a sus apoyos mediante empotramientos. Empotramiento.

Farkas, J., & Jármai, K. (2008). Seismic Resistant Design. Design and Optimization of Metal Structures, 27–32. https://doi.org/10.1533/9781782420477.27

Ministerio de desarrollo urbano y vivienda. (2015). Normativa Ecuatoriana de la construcción. Ecuador: NEC

Medina, E. (2016). 'Análisis comparativo de desplazamientos laterales y derivas entre edificaciones altas con sistemas aporticados y edificaciones altas con sistemas duales en zonas de alto riesgo sísmico [Graduation project]. Universidad Católica Andrés Bello.

Sánchez, P. C. & Arroba, P. V. (2019). Diseño de columnas, muros estructurales y diafragmas en hormigón armado. [Graduation project]. Universidad de Fuerzas Amadas ESPE.

Norma chilena NCh2745-2003. (2003). Obteined: studocu. https://www.studocu.com/cl/document/universidad-de-concepcion/ingenieria-de-la-construccion/nch2745-2003/11369431

Morocho, D., G. (2014). "Cálculo de la deriva de piso en un edificio de seis pisos altos y dos subterráneos con la utilización del CEC 2002 y NEC 2011 y su incidencia en los resultados finales [Structured independent research work prior to obtaining the degree of Civil Engineer]. Universidad Técnica de Ambato facultad de Ingeniería Civil y Mecánica carrera de Ingeniería Civil.

Loh, F. C., & Yeo, J. F. (1990). Bifid mandibular condyle. Oral surgery, oral medicine, oral pathology, 69(1), 24-27.

Vela, A. (2021). Análisis no lineal de estructuras regulares de hormigón armado ante eventos tsunamigénicos en Tonsupa-Esmeraldas [Articulo de investigación]. Universidad Politécnica Salesiana.

R. Aguiar, Evaluación rápida de la deriva máxima de piso para calcular la vulnerabilidad sísmica de estructuras, Monograph Series in Earthquake Engineering

Ruiz, D. M., Borrero, M. C., León, M. P., & Vacca, H. A. (1969). Estimación de los niveles de desempeño estructural y de la deriva inelástica de pórticos de concreto considerando la variabilidad de los materiales de Bogotá. Ingeniería Y Competitividad,

Reglamento colombiano de construcción sismo resistente. (2010). [Normative]. Ministerio de Ambiente, Vivienda y Desarrollo Territorial

Miguel, A., Cristian, J., & Mora Camilo. (2013). Hormigón Armado. Quito - Ecuador: Universidad Central del Ecuador

Manobanda, C. (2017). "Estudio del comportamiento del acero de refuerzo expuesto al fuego durante diferentes periodos de tiempo [Graduation project]. Universidad Técnica de Ambato.

Granda, P. (2017). Análisis de costos y proceso constructivo de una vivienda unifamiliar en mampostería confinada [Graduation project]. Universidad San Francisco de Quito.

Al-Ahmari, A., Nasr, E.A., Moiduddin, K., Anwar, S., Kindi, M. Al, Kamrani, A., 2015. A comparative study on the customized design of mandibular reconstruction plates using finite element method. Advances in Mechanical Engineering 7, 1–11. https://doi.org/10.1177/1687814015593890

Ananthan, S., Pertes, R.A., Bender, S.D., 2023. Biomechanics and Derangements of the Temporomandibular Joint. Dent. Clin. North Am. 67, 243–257. https://doi.org/10.1016/j.cden.2022.11.004

Borrás-Ferreres, J., Sánchez-Torres, A., Gay-Escoda, C., 2018. Bifid mandibular condyles: A systematic review. Med. Oral Patol. Oral Cir. Bucal 23, e672. https://doi.org/10.4317/medoral.22681

Burkhart, T.A., Andrews, D.M., Dunning, C.E., 2013. Finite element modeling mesh quality, energy balance and validation methods: A review with recommendations associated with the modeling of bone tissue. J. Biomech. https://doi.org/10.1016/j.jbiomech.2013.03.022

Ding, X., Liao, S., Zhu, X., Wang, H., Zou, B., 2015. Effect of orthotropic material on finite element modeling of completely dentate mandible. Mater. Des. 84, 144–153. https://doi.org/10.1016/j.matdes.2015.06.091

© 2026 by the author(s). Distributed under a Creative Commons CC BY license.

Preprints.org (www.preprints.org) | NOT PEER-REVIEWED | Posted: 9 May 2026 doi:10.20944/preprints202605.0561.v1

Falcinelli, C., Valente, F., Vasta, M., Traini, T., 2023. Finite element analysis in implant dentistry: State of the art and future directions. Dental Materials 39, 539–556. https://doi.org/10.1016/j.dental.2023.04.002

Gačnik, F., Ren, Z., Hren, N.I., 2014. Modified bone density-dependent orthotropic material model of human mandibular bone. Med. Eng. Phys. 36, 1684–1692. https://doi.org/10.1016/j.medengphy.2014.09.013

Geuzaine, C., Remacle, J., 2009. Gmsh: A 3-D finite element mesh generator with built-in pre- and post-processing facilities. Int. J. Numer. Methods Eng. 79, 1309–1331. https://doi.org/10.1002/nme.2579

Gregolin, R.F., Zavaglia, C.A. de C., Tokimatsu, R.C., Pereira, J.A., 2017. Biomechanical Stress and Strain Analysis of Mandibular Human Region from Computed Tomography to Custom Implant Development. Advances in Materials Science and Engineering 2017, 1–9. https://doi.org/10.1155/2017/7525897

Haghnegahdar, A.A., Bronoosh, P., Khojastepour, L., Tahmassebi, P., 2014. Prevalence of Bifid Mandibular Condyle in a Selected Population in South of Iran. J. Dent. 15, 156.

Hart, N.H., Nimphius, S., Rantalainen, T., Ireland, A., Siafarikas, A., Newton, R.U., 2017. Mechanical basis of bone strength: influence of bone material, bone structure and muscle action. J. Musculoskelet. Neuronal Interact. 17, 114–139.

Jing, J., Qu, A., Ding, X., Hei, Y., 2015. [Biomechanical analysis on healing process of sagittal fracture of the mandibular condyle after rigid fixation]. Shanghai Kou Qiang Yi Xue 24, 164–9.

Labib, R., Hussam, H., Gong, Z.-C., 2025. The Relationship between Bifid Mandibular Condyle and Temporomandibular Disorder. J Int Dent Med Res 18, 1601–1603.

Mańkowski, J., Piękoś, J., Dominiak, K., Klukowski, P., Fotek, M., Zawisza, M., Żach, P., 2021. A mandible with the temporomandibular joint—A new FEM model dedicated to strength and fatigue calculations of bonding elements used in fracture and defect surgery. Materials 14. https://doi.org/10.3390/ma14175031

Morgan, E.F., Unnikrisnan, G.U., Hussein, A.I., 2018. Bone Mechanical Properties in Healthy and Diseased States. Annu. Rev. Biomed. Eng. 20, 119. https://doi.org/10.1146/ANNUREV-BIOENG-062117-121139

Nogueira, C.B.P., Costa, F.W.G., Carvalho, F.S.R., Bezerra, T.P., Neto, I.C.P., Júnior, F.I. da S., Soares, E.C.S., 2025. The interaction between third molars and surrounding periapical tissues in mandibular stress distribution during high-impact trauma: a finite element study. Med. Oral Patol. Oral Cir. Bucal 30, 394–400. https://doi.org/10.4317/medoral.26954

Öhman-Mägi, C., Holub, O., Wu, D., Hall, R.M., Persson, C., 2021. Density and mechanical properties of vertebral trabecular bone—A review. JOR Spine 4. https://doi.org/10.1002/jsp2.1176

Rivera-Tapia, E.D., Avila-Vega, C., Lopez-Fajardo, G., Tapia-Bravo, V., Ilbay-Yupa, D., Mantilla, P., 2025. Assessing the clinical relevance of finite element models in MARPE-induced behaviour of craniofacial structures: a biomechanical review. J. Biomech. https://doi.org/10.1016/j.jbiomech.2025.113010

Scolaro, A., Khijmatgar, S., Rai, P.M., Falsarone, F., Alicchio, F., Mosca, A., Greco, C., Del Fabbro, M., Tartaglia, G.M., 2022. Efficacy of Kinematic Parameters for Assessment of Temporomandibular Joint Function and Disfunction: A Systematic Review and Meta-Analysis. Bioengineering 9, 269. https://doi.org/10.3390/bioengineering9070269

Sevinç Gül, S.N., Murat, F., Şensoy, A.T., 2025. Evaluation of Biomechanical Effects of Mandible Arch Types in All-on-4 and All-on-5 Dental Implant Design: A 3D Finite Element Analysis. J. Funct. Biomater. 16. https://doi.org/10.3390/jfb16040134

Shu, J., Luo, H., Zhang, Y., Liu, Z., 2021. 3D Printing Experimental Validation of the Finite Element Analysis of the Maxillofacial Model. Front. Bioeng. Biotechnol. 9, 694140. https://doi.org/10.3389/fbioe.2021.694140

Torres-Villar, C., Pacheco Muñoz, J., Maranillo, E., Ottone, N.E., 2025. Bone Mass, Microarchitecture, and Morphometric Insights on a Right Unilateral Bifid Mandibular Condyle: A Micro-CT Analysis Report and Literature Review. Diagnostics 15, 2440. https://doi.org/10.3390/diagnostics15192440

Valenzuela-Fuenzalida, J.J., Navarro, K. lle K., Urbina, P., Trujillo-Riveros, M., Nova-Baeza, P., Orellana-Donoso, M., Rodriguez-Luengo, M., Beccerra Farfan, A., Sanchis-Gimeno, J.A., 2023. Prevalence of the Bifid Mandibular Condyle and Its Relationship with Pathologies of the Temporomandibular Joint: A Systematic Review and Meta-Analysis. Diagnostics 13, 3282. https://doi.org/10.3390/diagnostics13203282

Widyastuti, A., Ratih, D.N., Siswomihardjo, W., Dharma, I.G.B.B., 2026. The influence of dental cavity on biomechanical stress and strain distribution: A finite element analysis. Journal of Conservative Dentistry and Endodontics 29, 145–149. https://doi.org/10.4103/JCDE.JCDE_991_25

© 2026 by the author(s). Distributed under a Creative Commons CC BY license.

Preprints.org (www.preprints.org) | NOT PEER-REVIEWED | Posted: 9 May 2026 doi:10.20944/preprints202605.0561.v1

World Medical Association, 2024. WMA Declaration of Helsinki – Ethical Principles for Medical Research Involving Human Participants – WMA – The World Medical Association [WWW Document]. URL https://www.wma.net/policies-post/wma-declaration-of-helsinki/ (accessed 3.3.26).

Yatabe, M., Zwijnenburg, A., Megens, C.C.E.J., Naeije, M., 1995. The Kinematic Center: A Reference for Condylar Movements. J. Dent. Res. 74, 1644–1648. https://doi.org/10.1177/00220345950740100401

Zengin, A.Z., Sumer, T., Çam, K., 2025. Assessment of temporomandibular joint morphology of bifid mandibular condyles: a cone beam computed tomography study. Folia Morphol. (Warsz). 84, 655–663. https://doi.org/10.5603/fm.104250

Zhao, S.G., Jiang, W. Bin, Liang, X.Y., Zhang, Y.F., Zhang, J.Z., Li, R.Q., Qin, S., Quan, Y.Y., Ding, K., Li, Y.B., Li, Z.Q., Chen, W., Liu, C.Y., 2025. Biomechanical features and fracture characteristics of mandible based on digital image correlation technique. BMC Oral Health 25, 1987. https://doi.org/10.1186/s12903-025-07386-0

Disclaimer/Publisher's Note: The statements, opinions and data contained in all publications are solely those of the individual author(s) and contributor(s) and not of MDPI and/or the editor(s). MDPI and/or the editor(s) disclaim responsibility for any injury to people or property resulting from any ideas, methods, instructions or products referred to in the content.

© 2026 by the author(s). Distributed under a Creative Commons CC BY license.